Flatband ferromagnetism and dispersion relations of spin-1 excitations in topological Hubbard models

Xiao-Fei Su,[1,2] Zhao-Long Gu,[1] Zhao-Yang Dong,[1] Shun-Li Yu,[1,3] and Jian-Xin Li[1,3]

[1] *National Laboratory of Solid State Microstructures and Department of Physics, Nanjing University, Nanjing 210093, China*
[2] *School of Physics and Electronic Information, Huaibei Normal University, Huaibei 235000, China*
[3] *Collaborative Innovation Center of Advanced Microstructures, Nanjing University, Nanjing 210093, China*

(Dated: June 8, 2018)

We study the spin-1 excitation spectra of the flatband ferromagnetic phases in topological Hubbard models. As a paradigm, we consider a quarter filled square lattice Hubbard model whose free part is the π flux model with topologically nontrivial and nearly-flat electron bands. The model Hamiltonian either explicitly breaks the time-reversal symmetry but preserves the spin $SU(2)$ rotation symmetry (Chern Hubbard model), or preserves the time-reversal symmetry but explicitly breaks the spin $SU(2)$ rotation symmetry (Z_2 Hubbard model). By using the numerical exact diagonalization method with a projection onto the lower nearly-flat electron band, we determine the critical Hubbard interaction strength upon which the ferromagnetic phase is stable, and elaborate the ferromagnetic spin-1 excitation spectra of the Chern Hubbard model and the Z_2 Hubbard model. Both spectra consist of collective modes (spin waves) and individual modes (Stoner continuum). For the Chern Hubbard model, the spin wave is gapless while for the Z_2 Hubbard model, the spin wave is gapped. Remarkably, for both cases, the nonflatness of the free electron bands introduces dips of the lower boundary of the Stoner continuum, and the scatterings between the Stoner continuum at these dips and the collective modes significantly reduce the latter's energy, which can lead to roton-like spin wave excitations. With the increase of this nonflatness, the energy of the induced roton-like modes goes down and finally touches zero, which results in the destabilization of the ferromagnetic phase.

I. INTRODUCTION

Electronic bands with nonzero topological indices reside on the center of a substantial amount of topological phenomena in condensed matter physics[1,2]. It was proposed in a pioneering work by Haldane[3] that a spinless fermionic model on a honeycomb lattice exhibits integer quantum Hall effect[4] without an external magnetic field. This model, serving as the first example of Chern insulator, breaks the time reversal symmetry with a complex next nearest neighbor hopping and is characterized by a nonzero Chern number[5]. Later, the concept was generalized to time reversal symmetric systems with spin-orbital coupling (SOC), such as the monolayer graphene[6,7] and HgTe/CdTe quantum wells[8,9]. The SOC there generates complex hopping terms similar to that proposed by Haldane but with opposite chiralities for electrons with up spins and down spins, resulting in the quantum spin Hall insulator characterized by a Z_2 index.

The lattice models with nontrivial band topology share much similarity with the two-dimensional electron gas (2DEG) under a strong magnetic field with Landau levels, e.g. the existence of topologically protected gapless edge states[3,6–11]. Thus more novel phases other than the Chern insulator or Z_2 insulator are expected when Coulomb interactions are taken into account, as is similar to the fractional quantum Hall effect[12,13] in the 2DEG with Landau levels. However, different from Landau levels, energy bands in lattice models usually have noneligible dispersions, which weakens the effect of Coulomb interactions. Therefore, in recent years, much effort has been devoted to the design and search of tight-binding models that host nearly-flat electron bands with nontrivial topology[14–20]. Analogous exotic phases, such as the fractional Chern insulator and fractional topological insulator were numerically verified to emerge in such nearly-flat topological bands when strong Coulomb interactions are turned on[18,21–24].

Another involved intriguing phenomenon arising from Coulomb repulsions in flat or nearly-flat bands is the itinerant ferromagnetism[25]. It was proved by Tasaki and Mielke that the ground state of an flat electron band with its filling factor not more than but sufficiently close to 1/2 is ferromagnetically ordered as long as an infinitesimal onsite Hubbard repulsion is present[26–28]. Afterwards this ferromagnetism was shown to be stable against small nonflatness of the electron bands if and only if the Hubbard interaction exceeds a critical value[29]. Spin wave excitations over this ferromagnetic ground state was also studied[30,31] and itinerant topological magnons has been reported quite recently[31].

The interplay between flatband ferromagnetism and nontrivial band topology enriches the related physics. In fact, ferromagnetism is essential in the generation of stable fractional Chern insulators in the proposals where the spin degrees of freedom of electrons are considered[14,23,24]. Furthermore, ferromagnetism can also lead to possible high-temperature quantum anomalous Hall effect (QAHE) when the nearly-flat topological band is half-filled[32]. In this paper, we focus on this ferromagnetism induced QAHE in nearly-flat topological bands. As a paradigm, we consider a square lattice Hubbard model whose free part is the π flux model with topologically nontrivial and nearly-flat electron bands. The model Hamiltonian either explicitly breaks the time-reversal symmetry but preserves the spin $SU(2)$ rotation symmetry (Chern Hub-

bard model), or preserves the time-reversal symmetry but explicitly breaks the spin $SU(2)$ rotation symmetry (Z_2 Hubbard model). When the model is quarter filled (or correspondingly, the lower nearly-flat band is half filled), the ground state is spin fully polarized due to the ferromagnetism and exhibits QAHE because of the nonzero Chern number of a single-spin band. Then the low energy physics is dominated by the one-spin-flip excitations. These spin-1 excitations has been studied by a generalized bosonization scheme where the interacting fermionic model is mapped to a free bosonic model describing spin-wave excitations at the harmonic approximation[33]. The ferromagnetism was shown to be stable against such spin wave excitations, which are gapless in the Chern Hubbard model and gapped in the Z_2 Hubbard model. However in this bosonization scheme, the free part of the electron model plays no role in the spin wave excitations other than contributing a global constant, which means it should fail due to the competition between the kinetic energy and potential energy of electrons when the nonflatness of the electron bands is not negligible[29]. What's worse, in a strictly local periodic tight-binding model, an energy band with a nonzero Chern number cannot be exactly flat[34]. Therefore it remains an open question on whether the ground state is stable against the spin-1 excitations and how the the nonflatness of the electron bands manifests itself in the spin-1 excitation spectra in such models.

To elucidate these questions, we adopt the numerical exact diagonalization method with a projection onto the lower nearly-flat band to take close investigations on the spin-1 excitations of the models. A critical Hubbard interaction strength is found for both the Chern Hubbard model and the Z_2 Hubbard model, upon which the ferromagnetic phase is stable. Furthermore the spin-1 excitation spectra are shown to consist of collective modes (spin waves) and individual modes (Stoner continuum). For the Chern Hubbard model, the spin wave is gapless while for the Z_2 Hubbard model, the spin wave is gapped. Remarkably, for both cases, the nonflatness of the free electron bands introduces dips of the lower boundary of the Stoner continuum, and the scatterings between the Stoner continuum at these dips and the collective modes significantly reduce the latter's energy, which can lead to roton-like spin wave excitations. With the increase of this nonflatness, the energy of the induced roton-like modes goes down and finally touches zero, which results in the destabilization of the ferromagnetic phase.

The rest of the paper is organized as follows. In Sec. II, we introduce the Chern Hubbard model and Z_2 Hubbard model studied in this paper, discuss the nontrivial band topology of their free parts, interpret the emergence of QAHE resulting from the interplay of flat-band ferromagnetism and nontrivial band topology, and formulate the exact diagonalization method with a projection onto the lower nearly-flat band on details. In Sec. III, we summarize the phase diagram and elaborate the spin-1 excitation spectra of both models. Section IV provides a summary and discussion.

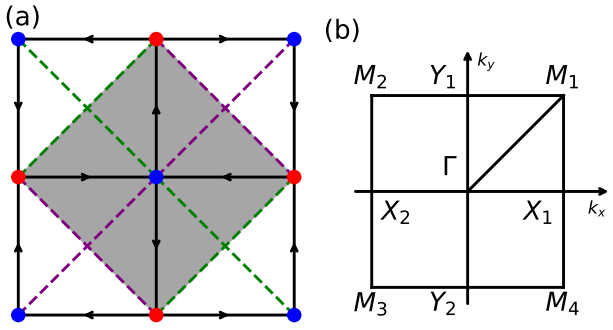

FIG. 1. (Color online) (a) Schematic representation of the π-flux model. Blue and red solid circles denote the A and B sublattices, respectively. The nearest-neighbor hopping amplitudes (solid black lines) are equal to $t_1 \exp[i\alpha(\sigma)\pi/4]$ ($\alpha(\sigma) = 1$ for the time-reversal-symmetry-breaking case and $\alpha(\sigma) = \pm 1$ for the time-reversal-symmetry-preserving case) along the direction of the arrows, the next-nearest-neighbor hopping amplitudes are equal to t_2 (dashed green lines) and $-t_2$ (dashed purple lines). The shaded area denotes the unit cell. (b) First Brillouin Zone. $\Gamma = (0,0)$, $X_{1,2} = (\pm\pi, 0)$, $Y_{1,2} = (0, \pm\pi)$, $M_{1,2,3,4} = (\pm\pi, \pm\pi)$.

II. MODEL AND METHOD

A. Introduction to model

We consider a generalized π-flux Hubbard model on the square lattice, whose Hamiltonian can be written as $H = H_0 + H_U$, where H_0 is the generalization with electron spin of the original spinless model proposed in Ref.[18],

$$H_0 = \sum_{\langle ij\rangle,\sigma} (t_1^{ij,\sigma} c_{i\sigma}^\dagger c_{j\sigma} + \text{H.c.}) + \sum_{\langle\langle ij\rangle\rangle,\sigma} (t_2^{ij} c_{i\sigma}^\dagger c_{j\sigma} + \text{H.c.}), \tag{1}$$

and H_U is the Hubbard interaction

$$H_U = U \sum_i n_{i\uparrow} n_{i\downarrow}. \tag{2}$$

Here, $c_{i\sigma}^\dagger (c_{i\sigma})$ creates (annihilates) a spin σ electron at site i, $n_{i\sigma}$ is the spin σ electron number operator at site i, $\langle ij\rangle$ denotes the nearest-neighbor (NN) bonds and $\langle\langle ij\rangle\rangle$ denotes the next-nearest-neighbor (NNN) bonds. As is shown in Fig. 1(a), the spin-dependent NN hopping amplitude $t_1^{ij,\sigma}$ and the spin-independent NNN hopping amplitude t_2^{ij} are given by

$$t_1^{ij,\sigma} = t_1 \exp\left[i(-1)^{\delta_{ij}^1} \alpha_\sigma \pi/4\right], \tag{3}$$

$$t_2^{ij} = t_2 (-1)^{\delta_{ij}^2}. \tag{4}$$

Here, $\delta_{ij}^1 = +1$ if the NN electron hopping is along the direction of the solid black arrow and $\delta_{ij}^1 = -1$ if along

the reversed direction. $\delta_{ij}^2 = +1$ if the NNN electron hopping is along the dashed green lines and $\delta_{ij}^2 = -1$ if along the dashed purple lines. The spin-dependent phase α_σ breaks the time-reversal symmetry but preserves the spin $SU(2)$ rotation symmetry if $\alpha_\uparrow = \alpha_\downarrow = +1$, whereas it preserves the time-reversal symmetry but breaks the spin $SU(2)$ rotation symmetry if $\alpha_\uparrow = +1$ and $\alpha_\downarrow = -1$.

Due to the complex NN hopping, each electron will acquire a π phase as it hops around a plaquette along the direction of the black arrows as indicated in Fig. 1(a). Therefore, H_0 describes free electrons hopping on a square lattice in the presence of a fictitious staggered π-flux pattern[35]. For the time-reversal-symmetry-breaking case, $\alpha_\uparrow = \alpha_\downarrow$, the flux experienced by spin-up electrons and spin-down electrons is the same, while for the time-reversal-symmetry-preserving case, $\alpha_\uparrow = -\alpha_\downarrow$, it is opposite.

B. Topology of free part

Gapped noninteracting fermionic systems can be topologically classified in the presence of symmetries by their Hamiltonians in the momentum space[36]. After the Fourier transformation, the free part H_0 of our model reads

$$H_0 = \sum_{\mathbf{k}\sigma} \psi_{\mathbf{k}\sigma}^\dagger h_{\mathbf{k}\sigma} \psi_{\mathbf{k}\sigma}, \tag{5}$$

where $\psi_{\mathbf{k}\sigma}^\dagger = (c_{A\mathbf{k}\sigma}^\dagger, c_{B\mathbf{k}\sigma}^\dagger)$ and

$$h_{\mathbf{k}\sigma} = \mathbf{D}_{\mathbf{k}\sigma} \cdot \boldsymbol{\tau}. \tag{6}$$

Here $\boldsymbol{\tau} = (\tau_1, \tau_2, \tau_3)$ is a 2×2 matrix vector, τ_1, τ_2, τ_3 are the three Pauli matrices for the sublattice degrees of freedom. The components of $\mathbf{D}_{\mathbf{k}\sigma}$ are given by

$$\begin{aligned} D_{1,\mathbf{k}} &= 2\sqrt{2} t_1 \cos\frac{k_x}{2} \cos\frac{k_y}{2}, \\ D_{2,\mathbf{k}} &= 2\sqrt{2} t_1 \alpha_\sigma \sin\frac{k_x}{2} \sin\frac{k_y}{2}, \\ D_{3,\mathbf{k}} &= 2t_2(\cos k_x - \cos k_y). \end{aligned} \tag{7}$$

H_0 can be diagonalized with the transformation

$$\begin{aligned} c_{A\mathbf{k}\sigma} &= \mu_{1,\mathbf{k}\sigma} d_{\mathbf{k}\sigma} + \mu_{2,\mathbf{k}\sigma} f_{\mathbf{k}\sigma}, \\ c_{B\mathbf{k}\sigma} &= \mu_{1,\mathbf{k}\sigma}^* f_{\mathbf{k}\sigma} - \mu_{2,\mathbf{k}\sigma}^* d_{\mathbf{k}\sigma}, \end{aligned} \tag{8}$$

where

$$\begin{aligned} \mu_{1,\mathbf{k}\sigma} &= \frac{D_{1,\mathbf{k}} - i\alpha_\sigma D_{2,\mathbf{k}}}{\sqrt{2D_{\mathbf{k}}(D_{\mathbf{k}} + D_{3,\mathbf{k}})}}, \\ \mu_{2,\mathbf{k}\sigma} &= \frac{D_{\mathbf{k}} + D_{3,\mathbf{k}}}{\sqrt{2D_{\mathbf{k}}(D_{\mathbf{k}} + D_{3,\mathbf{k}})}}, \end{aligned} \tag{9}$$

with $D_{\mathbf{k}} = \sqrt{D_{1,\mathbf{k}}^2 + D_{2,\mathbf{k}}^2 + D_{3,\mathbf{k}}^2}$. The diagonalized H_0 is given by

$$H_0 = \sum_{\mathbf{k}\sigma} \varepsilon_d(\mathbf{k}) c_{\mathbf{k}\sigma}^\dagger c_{\mathbf{k}\sigma} + \sum_{\mathbf{k}\sigma} \varepsilon_f(\mathbf{k}) f_{\mathbf{k}\sigma}^\dagger f_{\mathbf{k}\sigma}, \tag{10}$$

where $\varepsilon_d(\mathbf{k}) = -D_{\mathbf{k}}$, $\varepsilon_f(\mathbf{k}) = D_{\mathbf{k}}$. It can be seen that there exists a gap between the d band and f band when $t_1 \neq 0$ and $t_2 \neq 0$.

When there is a gap between the d band and the f band, these bands can be shown to be topologically nontrivial by calculating their Chern numbers[5] (for the time-reversal-symmetry breaking case) or Z_2 indices[7,37] (for the time-reversal-symmetry preserving case). The Chern number for a single spin component of the d band or the f band can be expressed in terms of the coefficients $D_{i,\mathbf{k}}$[1,2],

$$C_\sigma^{d/f} = \pm\frac{1}{4\pi} \int_{BZ} d^2k \, \hat{\mathbf{D}}_{\mathbf{k}\sigma} \cdot (\partial_{k_x} \hat{\mathbf{D}}_{\mathbf{k}\sigma} \times \partial_{k_y} \hat{\mathbf{D}}_{\mathbf{k}\sigma}) = \pm\alpha_\sigma, \tag{11}$$

with $\hat{\mathbf{D}}_{\mathbf{k}\sigma} \equiv \mathbf{D}_{\mathbf{k}\sigma}/D_{\mathbf{k}}$.

When the system breaks the time-reversal symmetry, i.e. $\alpha_\uparrow = \alpha_\downarrow = 1$, $C_\uparrow^d = C_\downarrow^d = 1$ and $C_\uparrow^f = C_\downarrow^f = -1$, the total Chern number of the d band is $C^d = C_\uparrow^d + C_\downarrow^d = 2$. Therefore, the ground state of H_0 will be a noninteracting Chern insulator and exhibits quantum anomalous Hall effect(QAHE) when the lower d band is fully filled. When the system preserves the time-reversal symmetry, i.e. $\alpha_\uparrow = -\alpha_\downarrow = 1$, $C_\uparrow^d = -C_\downarrow^d = 1$ and $C_\uparrow^f = -C_\downarrow^f = -1$, the total Chern number of the d band is zero. However, the Z_2 index, which is defined as

$$\nu = \frac{1}{2}(C_\uparrow - C\downarrow) \mod 2, \tag{12}$$

of the d band is 1 and nontrivial. As a consequence, the the ground state of H_0 will be a noninteracting Z_2 insulator and exhibits quantum spin Hall effect(QSHE) when the lower d band is fully filled.

C. Emergence of QAHE in half-filled nearly-flat topological bands

For a free fermionic system hosting an energy band with a nonzero Chern number or Z_2 index, the distinguished phenomenon resulting from this nontrivial band topology, such as QAHE or QSHE, only manifests itself when the topological band is fully filled. At any fractional filling, the ground state of such a system will be a trivial metal. Intriguingly, when the Coulomb interactions between electrons step in, the physics of the nontrivial band topology becomes more involved, especially when the band is nearly flat so that the effects of the Coulomb interactions are highly enhanced. Combined with strong Coulomb interactions, nontrivial topological phases can emerge from fractionally filled topological bands. In this article, we are interested in half-filled strongly-correlated nearly-flat topological bands where QAHE can arise[18,33]. The essence for the occurrence of this nontrivial phase is the emergence of itinerant ferromagnetism on nearly-flat bands[25], which fully polarizes all the electron spins. Therefore only one spin component of the topological band will be fully filled exactly, which leads to QAHE due

to the nonzero Chern number of that spin component of the band.

The Chern Hubbard model and Z_2 Hubbard model on square lattice described above serve as the paradigm, where half filling of the lower electron band corresponds to quarter filling of the whole system because of the existence of AB sublattices. When t_2/t_1 takes values in a selected region, the d band and f band are quite flat in that the flatness ratio Δ/W, which is defined as the ratio between the electron gap Δ between these two bands and the bandwidth W of the lower band, can be as large as 4.83[18,33]. In Ref.[18], the quarter filled Z_2 Hubbard model was studied and all spin excitations were shown to be gapped in the flatband limit, which is essential for a possible high-temperature realization of QAHE. In Ref.[33], both models at quarter filling were considered and a generalized bosonization scheme was developed to study the spin-1 excitation spectra. However, in their bosonization scheme, the free part H_0 of the Hamiltonian only contributes a constant to the spectra, thus it cannot capture the physics caused by the nonflatness of the topological electron bands, which is unavoidable because an energy band with a nonzero Chern number in a strictly local periodic tight binding model cannot be exactly flat[34]. The spin-1 excitations, as the dominant low-energy excitations, deserves closer investigations to understand the stability of such phases and the physics related to the nonflatness of the topological bands. In the next subsection, we will introduce the exact diagonalization method with a projection onto the lower nearly-flat electron band to elucidate these questions.

D. Exact diagonalization with projection

Exact diagonalization method with a projection onto the low-energy Hilbert space bas been widely applied to systems that host flat or nearly-flat energy bands[18,22,23,31–33]. This approach ignores the band mixing of electrons and applies when the Coulomb interaction is small compared to the energy gap of the electron bands.

For the model we study in this article, the relevant low-energy subspace is the lower electron band, i.e. the d band. Let P denote the corresponding projector, then the Hamiltonian after the projection is

$$P^\dagger H P = \sum_{\mathbf{k}\sigma} \varepsilon_d(\mathbf{k}) d^\dagger_{\mathbf{k}\sigma} d_{\mathbf{k}\sigma} + \frac{U}{N} \sum_{a=1,2} \sum_{\mathbf{k}\mathbf{k}'\mathbf{q}} (\mu^*_{a,\mathbf{k}+\mathbf{q}\uparrow} \mu^*_{a,\mathbf{k}'-\mathbf{q}\downarrow} \mu_{a,\mathbf{k}'\downarrow} \mu_{a,\mathbf{k}\uparrow}) d^\dagger_{\mathbf{k}+\mathbf{q}\uparrow} d^\dagger_{\mathbf{k}'-\mathbf{q}\downarrow} d_{\mathbf{k}'\downarrow} d_{\mathbf{k}\uparrow}. \tag{13}$$

Let $|\mathrm{FM}\rangle$ denote the spin-up fully polarized state on the d band,

$$|\mathrm{FM}\rangle = \prod_{\mathbf{k}\in \mathrm{FBZ}} d^\dagger_{\mathbf{k}\uparrow} |0\rangle, \tag{14}$$

where FBZ denotes the first Brillouin zone [see Fig. 1(b)] and $|0\rangle$ is the fermion vaccum. Then the basis of the spin-1 excitations with a center-of-mass momentum $\mathbf{q}$ over this reference state can be written as

$$|\mathbf{k}_i\rangle_{\mathbf{q}} = d^\dagger_{\mathbf{k}_i-\mathbf{q}\downarrow} d_{\mathbf{k}_i\uparrow} |\mathrm{FM}\rangle. \tag{15}$$

Here $d^\dagger_{\mathbf{k}_i-\mathbf{q}\downarrow}$ creates a spin-down electron with momentum $\mathbf{k}_i - \mathbf{q}$ and $d_{\mathbf{k}_i\uparrow}$ annihilates a spin-up electron with momentum $\mathbf{k}_i$. Therefore this basis labels a spin-1 scattering channel with the index $\mathbf{k}_i$. Thus the dimension of this Hilbert space scales linearly with respect to the number of electron momentums[31], and a much larger system can be numerically accessed than the usual exact diagonalization without projection, which enables us to analyze the properties of the spin-1 excitation spectra at the whole first Brillouin zone rather than some restricted discrete points solely. The matrix element of the projected Hamiltonian on this spin-1 excitation basis can be easily obtained after some algebra,

$$\begin{aligned} {}_{\mathbf{q}}\langle \mathbf{k}_j | P^\dagger H P | \mathbf{k}_i \rangle_{\mathbf{q}} = & \left[\varepsilon_d(\mathbf{k}_i - \mathbf{q}) - \varepsilon_d(\mathbf{k}_i) + \frac{U}{N} \sum_{a=1,2} \sum_{\mathbf{p}\neq\mathbf{k}_i} |\mu_{a,\mathbf{p}\uparrow}|^2 \, |\mu_{a,\mathbf{k}_i-\mathbf{q}\downarrow}|^2 \right] \delta_{\mathbf{k}_j,\mathbf{k}_i} \\ & - \frac{U}{N} \sum_{a=1,2} \mu^*_{a,\mathbf{k}_i\uparrow} \mu_{a,\mathbf{k}_j\uparrow} \mu^*_{a,\mathbf{k}_j-\mathbf{q}\downarrow} \mu_{a,\mathbf{k}_i-\mathbf{q}\downarrow} \left(1 - \delta_{\mathbf{k}_j,\mathbf{k}_i}\right). \end{aligned} \tag{16}$$

Here $\delta_{\mathbf{k}_j,\mathbf{k}_i}$ is the Kronecker delta function. Then the full spin-1 excitation spectra can be obtained by the diagonalization of the matrix whose elements are defined by Eq. (16). It is noted that $|\mathrm{FM}\rangle$ is the true ground state only if the whole spin-1 excitation spectra have no negative eigen energies. Thus we can use this as the criterion

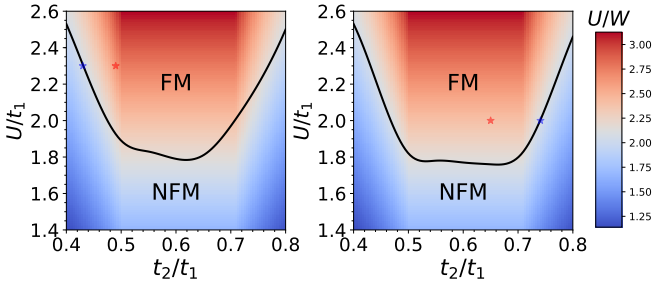

FIG. 2. (Color online) Phase diagram of the quarter-filled (a) Chern Hubbard model and (b) Z_2 Hubbard model. The colormap represents the ratio U/W of the lower electron band, where U is the Hubbard interaction strength and W is the lower electron bandwidth. Red stars in (a) and (b) mark the parameters used in Fig. 3 and Fig. 5(a), respectively. Blue stars in (a) and (b) mark the parameters used in Fig. 4. and Fig. 5(b), respectively.

to determine the destabilization point of the ferromagnetic phase.

We also want to give some remarks on the flatband limit in the framework of this method. The free part $h^{\text{flat}}_{\mathbf{k}\sigma}$ of the Hamiltonian in the flatband limit is defined as

$$h^{\text{flat}}_{\mathbf{k}\sigma} = \frac{h_{\mathbf{k}\sigma}}{|\varepsilon_d(\mathbf{k})|} = \hat{\mathbf{D}}_{\mathbf{k}\sigma} \cdot \tau. \tag{17}$$

$h^{\text{flat}}_{\mathbf{k}\sigma}$ shares the same eigenfunctions with $h_{\mathbf{k}\sigma}$ but has exactly-flat energy bands with the eigenvalues being ± 1. $h^{\text{flat}}_{\mathbf{k}\sigma}$, together with the Hubbard interaction H_U, defines the flatband limit of the original Hamiltonian. To approach this limit, long-range hopping terms in the real space must be included[18]. To elaborate the physics related to the nonflatness of the d band, we also calculated the spin-1 excitation spectra in the flatband limit for comparison. This can be done by simply ignoring the $[\varepsilon_d(\mathbf{k}_i - \mathbf{q}) - \varepsilon_d(\mathbf{k}_i)]\,\delta_{\mathbf{k}_j,\mathbf{k}_i}$ term in Eq. (16), because of the same eigenfunctions shared by $h^{\text{flat}}_{\mathbf{k}\sigma}$ and $h_{\mathbf{k}\sigma}$.

III. NUMERICAL RESULTS

The phase diagrams of the quarter-filled Chern Hubbard model and Z_2 Hubbard model are shown in Fig. 2. Here, the colormap represents the ratio of the Hubbard interaction strength U over the lower electron bandwidth W. FM denotes the ferromagnetic phase and NFM denotes the non-ferromagnetic phase. As is discussed in Sec. II D, the phase boundary is determined as the onset point of U below which negative spin-1 excitation spectra appear. It is clear that a critical Hubbard interaction strength is needed to maintain the ferromagnetically ordered ground state when the electron band has finite nonflatness. This observation is expected as a result from the competition between the kinetic energy and the potential energy of the electrons, as a fully spin-polarized state minimizes the energy of Hubbard interactions but cost more energy when the electron band disperses. An intriguing fact about the phase diagrams is that the phase boundaries always lie near the contour line with $U/W = 2.0$.

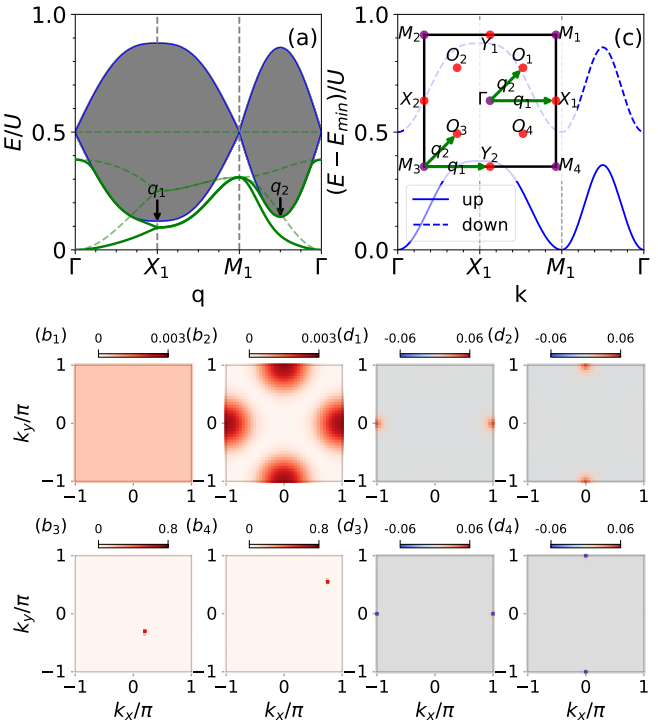

FIG. 3. (Color online) (a) Spin-1 excitation spectra of the Chern Hubbard model in the FM phase. Green solid lines denote the spin waves and the grey regions denote the Stoner continuum. Green dashed lines represent the corresponding spectra in the flatband limit. Blue solid lines denote the upper and lower boundaries of the Stoner continuum determined by the split band picture shown in (c). Black arrows mark the local minima of the Stoner continuum. (b) Spectral weights for the lowest four eigen levels of the spin-1 excitation spectra with the center-of-mass momentum $\mathbf{q} = (0, 0)$. (c) Illustration of the splitting of the lower electron bands for up spins (blue solid line) and down spins (blue dashed line) in the presence of ferromagnetism of the Chern Hubbard model. Inset shows the positions of the corresponding local maxima (red solid circles) of the spin-up bands and local minima (purple solid circles) of the spin-down bands in the first Brillouin zone. Green arrows denote the corresponding scattering channels of the dips of the Stoner continuum marked in (a). (d) Differences of the spectral weights subtracted by those in the flatband limit for the lowest four eigen levels of the spin-1 excitation spectra with the center-of-mass momentum $\mathbf{q} = (\pi, 0)$. The parameters are $t_1 = 1.0$, $t_2 = 0.49$ and $U = 2.3$.

A. Chern Hubbard model

To gain a comprehensive understanding of the physics observed above, the spin-1 excitation spectra along a high

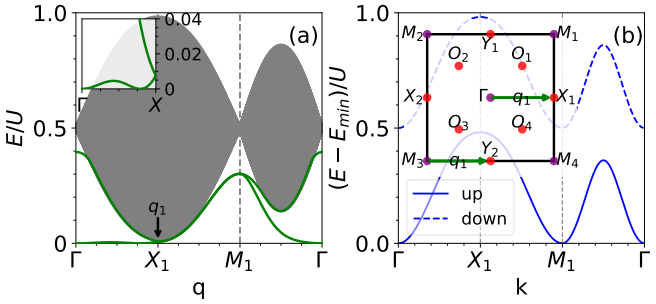

FIG. 4. (Color online) (a) Spin-1 excitation spectra of the Chern Hubbard model at the FM/NFM phase boundary. Black arrow marks the minimum of the Stoner continuum. Inset shows its low-energy part along Γ-X path with an amplified resolution. (b) Illustration of the splitting of the lower electron bands of the Chern Hubbard model. Inset shows the positions of the corresponding local maxima (red solid circles) of the spin-up bands and local minima (purple solid circles) of the spin-down bands in the first Brillouin zone. Green arrows denote the corresponding scattering channels of the minimum of the Stoner continuum marked in (a). The parameters are $t_1 = 1.0$, $t_2 = 0.43$ and $U = 2.3$.

symmetry path in the first Brillouin zone of the quarter-filled Chern Hubbard model with two different t_2 values are plotted in Fig. **??**(a)-(b) as the green solid lines and the shaded areas. For a comparison, the spectra for those in the corresponding flat-band limit are shown as the green dashed lines as well. Apparently, for both the original model and the flat-band limit model, the spectra consist of two types of modes: the low-lying ones exhibiting well-defined band structures and the high-energy ones forming a continuum. The former are identified as the magnons with an acoustic branch and an optical branch while the latter are identified as the Stoner continuum. At Γ point, the acoustic magnon band is gapless, which is the character of a ferromagnetic excitation with the Goldstone mode as the result of the spontaneous spin $SU(2)$ symmetry breaking. Remarkably,

B. Topological Hubbard model

IV. SUMMARY AND DISCUSSION

ACKNOWLEDGMENTS

This work was supported by the National Natural Science Foundation of China (11774152) and National Key Projects for Research and Development of China (Grant No. 2016YFA0300401).

X.-F. S. and Z.-L. G. contributed equally to this work.

[1] M. Z. Hasan and C. L. Kane, Rev. Mod. Phys. **82**, 3045 (2010).
[2] X.-L. Qi and S.-C. Zhang, Rev. Mod. Phys. **83**, 1057 (2011).
[3] F. D. M. Haldane, Phys. Rev. Lett. **61**, 2015 (1988).
[4] K. v. Klitzing, G. Dorda, and M. Pepper, Phys. Rev. Lett. **45**, 494 (1980).
[5] D. J. Thouless, M. Kohmoto, M. P. Nightingale, and M. den Nijs, Phys. Rev. Lett. **49**, 405 (1982).
[6] C. L. Kane and E. J. Mele, Phys. Rev. Lett. **95**, 226801 (2005).
[7] C. L. Kane and E. J. Mele, Phys. Rev. Lett. **95**, 146802 (2005).
[8] B. A. Bernevig, T. L. Hughes, and S.-C. Zhang, Science **314**, 1757 (2006).
[9] M. König, S. Wiedmann, C. Brüne, A. Roth, H. Buhmann, L. W. Molenkamp, X.-L. Qi, and S.-C. Zhang, Science **318**, 766 (2007).
[10] R. B. Laughlin, Phys. Rev. B **23**, 5632 (1981).
[11] B. I. Halperin, Phys. Rev. B **25**, 2185 (1982).
[12] D. C. Tsui, H. L. Stormer, and A. C. Gossard, Phys. Rev. Lett. **48**, 1559 (1982).
[13] R. B. Laughlin, Phys. Rev. Lett. **50**, 1395 (1983).
[14] E. Tang, J.-W. Mei, and X.-G. Wen, Phys. Rev. Lett. **106**, 236802 (2011).
[15] F. Wang and Y. Ran, Phys. Rev. B **84**, 241103 (2011).
[16] K. Sun, Z. Gu, H. Katsura, and S. Das Sarma, Phys. Rev. Lett. **106**, 236803 (2011).
[17] Y.-F. Wang, Z.-C. Gu, C.-D. Gong, and D. N. Sheng, Phys. Rev. Lett. **107**, 146803 (2011).
[18] T. Neupert, L. Santos, C. Chamon, and C. Mudry, Phys. Rev. Lett. **106**, 236804 (2011).
[19] M. Trescher and E. J. Bergholtz, Phys. Rev. B **86**, 241111 (2012).
[20] S. Yang, Z.-C. Gu, K. Sun, and S. Das Sarma, Phys. Rev. B **86**, 241112 (2012).
[21] D. Sheng, Z.-C. Gu, K. Sun, and L. Sheng, Nat. Commun. **2**, 389 (2011).
[22] N. Regnault and B. A. Bernevig, Phys. Rev. X **1**, 021014 (2011).
[23] T. Neupert, L. Santos, S. Ryu, C. Chamon, and C. Mudry, Phys. Rev. B **84**, 165107 (2011).
[24] Z. Liu, E. J. Bergholtz, H. Fan, and A. M. Läuchli, Phys. Rev. Lett. **109**, 186805 (2012).
[25] H. Tasaki, Prog. Thoer. Phys. **99**, 489 (1998).
[26] H. Tasaki, Phys. Rev. Lett. **69**, 1608 (1992).
[27] A. Mielke, Phys. Lett. A **174**, 443 (1993).
[28] A. Mielke and H. Tasaki, Commun. Math. Phys **158**, 341 (1993).
[29] H. Tasaki, Phys. Rev. Lett. **73**, 1158 (1994).
[30] K. Kusakabe and H. Aoki, Phys. Rev. Lett. **72**, 144 (1994).
[31] X.-F. Su, Z.-L. Gu, Z.-Y. Dong, and J.-X. Li, arXiv:1801.05255 (2018).
[32] T. Neupert, L. Santos, S. Ryu, C. Chamon, and C. Mudry, Phys. Rev. Lett. **108**, 046806 (2012).
[33] R. L. Doretto and M. O. Goerbig, Phys. Rev. B **92**, 245124 (2015).

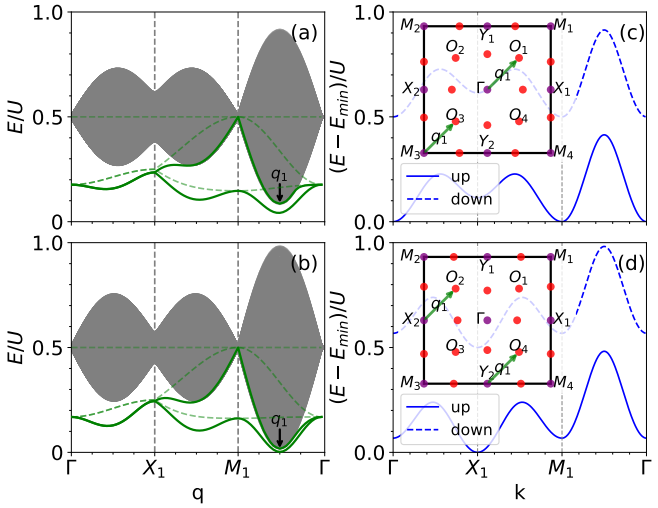

FIG. 5. (Color online) (a) and (b): Spin-1 excitation spectra of the Z_2 Hubbard model. Green solid lines denote the spin waves and the grey regions denote the Stoner continuum. Green dashed lines represent the corresponding spectra in the flatband limit. Black arrows mark the minima of the Stoner continuum. (c) and (d): Illustration of the splitting of the lower electron bands of the Z_2 Hubbard model. Insets show the positions of the corresponding local maxima (red solid circles) of the spin-up bands and local minima (purple solid circles) of the spin-down bands in the first Brillouin zone. Green arrows denote the corresponding scattering channels of the minima of the Stoner continuum marked in (a) and (b). $t_2 = 0.65$ for (a) and (c) and $t_2 = 0.741$ for (b) and (d). Other parameters are fixed at $t_1 = 1.0$, $U = 2.3$.

[34] L. Chen, T. Mazaheri, A. Seidel, and X. Tang, J. Phys. A: Math. Theor. **47**, 152001 (2014).

[35] X. G. Wen, F. Wilczek, and A. Zee, Phys. Rev. B **39**, 11413 (1989).

[36] A. P. Schnyder, S. Ryu, A. Furusaki, and A. W. W. Ludwig, Phys. Rev. B **78**, 195125 (2008).

[37] D. N. Sheng, Z. Y. Weng, L. Sheng, and F. D. M. Haldane, Phys. Rev. Lett. **97**, 036808 (2006).